Journal of Sound and Vibration (2001) **241**(2), 283–295
doi:10.1006/jsvi.2000.3296, available online at http://www.idealibrary.com on IDEAL®

ACOUSTIC RESPONSE OF A NON-CIRCULAR CYLINDRICAL ENCLOSURE USING CONFORMAL MAPPING

P. THAMBURAJ AND J. Q. SUN

Department of Mechanical Engineering, University of Delaware, Newark, DE 19716, *U.S.A.*

(*Received* 24 *May* 2000, *and in final form* 7 *August* 2000)

This paper presents a study of the free and forced interior acoustic response of a finite uniform cylindrical shell. The cross-section of the shell is a square with rounded corners. Conformal mapping is used to map the physical domain onto a circular cylindrical domain. The acoustic response is obtained in the circular domain by using the Rayleigh–Ritz method in conjunction with a variational principle. Numerical simulation results are presented showing the mode shapes and the forced pressure distribution at various frequencies.

1. INTRODUCTION

Large global transport aircraft will be required both militarily and commercially in the future. The fuselages of these aircraft will most likely involve cross-sections with shapes other than circular. Fuselage cross-sections involving straight elements for the keel, crown and sides connected by rounded corners are of particular importance. With such cross-sections, the bending stresses due to fuselage loads can be large. Minimization of the bending stresses has been studied quite extensively in the past [1–3]. In the current work, the internal acoustic response of a fuselage with such a cross-section is analyzed.

An example of an existing aircraft with such a cross-section is the Dornier 228. The structure and cavity modes have been computed for this aircraft using a finite element analysis [4]. Experiments have also been done to measure the noise levels inside the fuselage during flight. The current work applies the method of conformal mapping to compute the free and forced acoustic responses of the air inside the structure. The non-circular domain is mapped to the interior of a unit circle by a conformal mapping. The system is then analyzed in the circular domain and the solution is mapped back onto the physical domain. Use of conformal mapping is widespread in various areas. Examples of stress analysis of elastic plates with irregular geometry can be found in references [5–7]. Vibration analysis of non-circular plates and shells using conformal mapping has also been studied [8–11]. The acoustic responses in irregularly shaped domains have been investigated in references [12–15]. The acoustic solutions of fluid waveguides with complicated cross-sections have been presented in references [16–18]. The method of conformal mapping has been used by DiPerna and Stanton in the investigation of sound scattering by cylinders with non-circular cross-sections [19]. The emphasis of this work is to study the interior acoustic response of an aircraft fuselage with a non-circular cross-section by using conformal mapping in conjunction with a variational formulation. This paper studies both the free and forced acoustic responses in the enclosure. Experimental validation of the prediction, however, is beyond the scope of this preliminary study.

0022-460X/01/120283 + 13 $35.00/0

The paper is organized as follows. A variational principle for interior acoustic problems and the conformal mapping for the cylindrical shell with a non-circular cross-section are presented in section 2. The Rayleigh–Ritz method for the acoustic solution is outlined. In section 3, the mode shapes of the acoustic response for the non-circular cylindrical interior are presented. The pressure distribution on the boundary of the cylinder subject to an interior acoustic excitation is also studied.

2. PROBLEM STATEMENT

2.1. VARIATIONAL PRINCIPLE

The variational approach has been used in the analysis of structural-acoustic problems by Gladwell [20, 21]. For our problem, the special geometry also calls for the use of a variational formulation. We have found that although the acoustic pressure $p(\mathbf{r}, t)$ is the physical variable of interest, it is more convenient to consider the variational formulation in terms of the acoustic velocity potential $\Phi(\mathbf{r}, t)$. These two terms are related through Bernoulli's equation [22, 23]

$$p(\mathbf{r}, t) = -\rho \frac{\partial \Phi(\mathbf{r}, t)}{\partial t}, \tag{1}$$

where ρ is the density of the air. The kinetic and potential energies of the air within the shell can be written as

$$T = \frac{1}{2} \int_{D(\mathbf{r})} \rho \mathbf{v}^2 \, \mathrm{d}v = \frac{1}{2} \int_{D(\mathbf{r})} \rho \, (\nabla \Phi)^2 \, \mathrm{d}v, \tag{2}$$

$$V = \frac{1}{2} \int_{D(\mathbf{r})} \frac{p(\mathbf{r}, t)^2}{\rho c_0^2} \, \mathrm{d}v = \frac{1}{2} \int_{D(\mathbf{r})} \frac{\rho}{c_0^2} \left(\frac{\partial \Phi}{\partial t} \right)^2 \mathrm{d}v, \tag{3}$$

where $\mathbf{v}$ is the particle velocity, c_0 is the speed of sound in the air and $\mathrm{d}v$ is the elemental volume in the physical domain $D(\mathbf{r})$. A volume displacement density $q(\mathbf{r}, t)$ in the enclosure is considered as the excitation. The virtual work done by this source is given as

$$\delta W = -\int_{D(\mathbf{r})} \delta p(\mathbf{r}, t) q(\mathbf{r}, t) \, \mathrm{d}v = \int_{D(\mathbf{r})} \rho \delta \left(\frac{\partial \Phi}{\partial t} \right) q \, (\mathbf{r}, t) \, \mathrm{d}v. \tag{4}$$

Equations (2) and (3) show that the kinetic energy T is related to $(\nabla \Phi)^2$ and the potential energy V to $\dot{\Phi}^2$. This is opposite to the results commonly seen in structural analysis. This reversal is the reason that the virtual work in equation (4) is given by a product of the virtual force and the displacement. In structural analysis, the virtual work is a product of the external force and the virtual displacement [24].

2.2. CONFORMAL MAPPING

Consider the rigid-wall cylinder with a cross-section shown in Figure 1. Let the cross-section of the physical domain $D(\mathbf{r})$ be in the complex η-plane. This cross-section is mapped onto a unit circle in the complex ξ-plane by the following conformal mapping

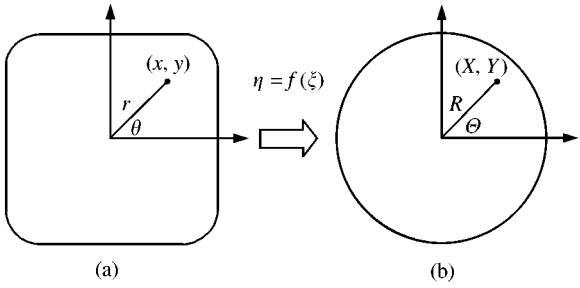

Figure 1. Conformal mapping from (a) the physical domain (η-plane) to (b) the circular domain (ξ-plane).

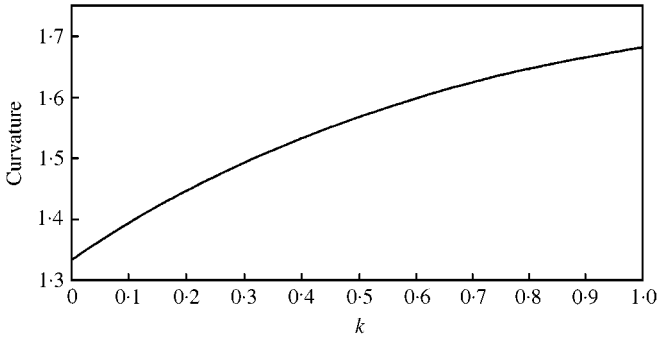

Figure 2. The variation of the curvature of the cross-section at the corners with the parameter k.

[5, 8, 9]:

$$\eta = f(\xi) = aL_t\left[\xi - \frac{1+k}{25}\xi^5 + \frac{k}{81}\xi^9\right]. \tag{5}$$

The parameter k in equation (5) can be varied to control the curvature at the corners of the square. The variation of the curvature with the parameter k is shown in Figure 2. The width of the square is $2a$ and $L_t = \frac{25}{24}$ is a transformation constant.

Let $\eta = re^{j\theta} = x + jy$, where (r, θ) and (x, y) are the polar and the Cartesian co-ordinates of the cross-section. Since the mapping is only for the cross-section, it is a two-dimensional mapping and the axial co-ordinate of the cylindrical interior remains unchanged. Let $\xi = Re^{j\Theta} = X + jY$, where (R, Θ) and (X, Y) are the polar and Cartesian co-ordinates, respectively, of the cross-section in the ξ-plane. Hence, the total mapping for the three-dimensional interior is from $\mathbf{r} = (x, y, z) = (r, \theta, z)$ to $\mathbf{R} = (X, Y, z) = (R, \Theta, z)$. Note that z is the axial co-ordinate in both domains. Hamilton's principle for the present problem in the transformed domain reads as

$$\begin{aligned} 0 = \int_{t_2}^{t_2}\int_{D(\mathbf{R})}\Bigg[&-\left(\left|\frac{d\xi}{d\eta}\right|^2 \nabla_\xi^2\Phi(\mathbf{R}) + \frac{\partial^2\Phi(\mathbf{R})}{\partial z^2}\right) + \frac{1}{c_0^2}\frac{\partial^2\Phi(\mathbf{R})}{\partial t^2} - \frac{\partial q(\mathbf{R},t)}{\partial t}\Bigg] \\ &\times \rho\delta\Phi(\mathbf{R})J(\mathbf{R})\,\mathrm{d}v(\mathbf{R})\,\mathrm{d}t \\ &+ \int_{D(\mathbf{R})}\left[\frac{1}{c_0^2}\frac{\partial\Phi(\mathbf{R})}{\partial t} - q(\mathbf{R},t)\right]\rho\delta\Phi(\mathbf{R})\Bigg|_{t_1}^{t_2} J(\mathbf{R})\,\mathrm{d}v(\mathbf{R}) \\ &+ \int_{t_1}^{t_2}\int_{S(\mathbf{R})}\frac{\partial\Phi(\mathbf{R})}{\partial n(\eta)}\,\rho\delta\Phi(\mathbf{R})\,J(\mathbf{R})\,\mathrm{d}S(\mathbf{R})\,\mathrm{d}t, \end{aligned} \tag{6}$$

where $J(\mathbf{R})$ is the Jacobian of the three-dimensional mapping and $dv(\mathbf{R})$ is the elemental volume in the transformed domain. The directional derivative $\partial\Phi(\mathbf{R})/\partial n(\eta)$ is along the outward normal to the surface $S(\mathbf{R})$. The governing inhomogeneous wave equation in the transformed domain can be derived from equation (6) [16–18]:

$$\left|\frac{d\xi}{d\eta}\right|^2 \nabla_\xi^2 \Phi(\mathbf{R}) + \frac{\partial^2\Phi(\mathbf{R})}{\partial z^2} - \frac{1}{c_0^2}\frac{\partial^2\Phi(\mathbf{R})}{\partial t^2} = -\frac{\partial q(\mathbf{R},t)}{\partial t}, \tag{7}$$

where ∇_ξ^2 is the two-dimensional Laplace operator in the ξ-plane, and

$$\begin{aligned}\left|\frac{d\xi}{d\eta}\right|^2 = \Bigg[(aL_t)^2\Bigg(1 - 10R^4\left(\frac{1+k}{25}\right)\cos(4\Theta) \\ + 18R^8\left(\frac{k}{81}\right)\cos(8\Theta) + 25R^8\left(\frac{1+k}{25}\right)^2 \\ - 90R^{12}\left(\frac{1+k}{25}\right)\left(\frac{k}{81}\right)\cos(4\Theta) + 81R^{16}\left(\frac{k}{81}\right)^2\Bigg)\Bigg]^{-1}.\end{aligned} \tag{8}$$

When the transformation is an identity, $|d\xi/d\eta| = 1$, and equation (7) becomes the well-known wave equation. Because of the complex coupling between the R and Θ co-ordinates in $|d\xi/d\eta|^2$, the method of separation of variables is not applicable to equation (7).

An important property of conformal mapping is that the relative angles are preserved [25]. In particular, the direction of the normal to the surface is also preserved. The directional derivatives along the normal of the curved surface of the shell in the two domains are related as

$$\frac{\partial\Phi(\mathbf{R})}{\partial n(\xi)} = \frac{1}{|f'(\xi)|}\frac{\partial\Phi(\mathbf{R})}{\partial n(\eta)} \quad \text{at } R = 1. \tag{9}$$

This ensures that the rigid-wall boundary condition is preserved in both domains:

$$\frac{\partial\Phi(\mathbf{r})}{\partial n(\eta)} = 0, \quad \mathbf{r} \in S(\mathbf{r}) \Rightarrow \frac{\partial\Phi(\mathbf{R})}{\partial n(\xi)} = 0, \quad \mathbf{R} \in S(\mathbf{R}). \tag{10}$$

Since the mapping of the z-co-ordinate is identity, the boundary conditions in the z direction on the rigid end caps at $z = 0$ and L are also unchanged by the transformation, where L is the length of the cylinder.

The solutions to the present acoustic problem can be solved in the transformed domain by using either the Rayleigh–Ritz or Galerkin method. Both these methods are essentially equivalent in terms of accuracy and convergence of the solution [24]. In this paper, the solutions are obtained with the Rayleigh–Ritz method.

2.3. RAYLEIGH–RITZ METHOD

Because of the boundary condition (10), the acoustic modes for the circular cylindrical domain are comparison functions for the present acoustic problem governed by equation

(7) [24]. The velocity potential in the transformed domain can then be written as

$$\Phi(R, \Theta, z, t) = \sum_{m=0}^{M} \sum_{n=-N}^{N} \sum_{p=1}^{P} \phi_{mnp}(t)\psi_{mnp}(R, \Theta, z), \tag{11}$$

$$\psi_{mnp}(R, \Theta, z) = \mathrm{J}_n(k_{np}R)\cos\frac{m\pi z}{L}\exp(\mathrm{j}n\Theta),$$

where $\phi_{mnp}(t)$ is the expansion coefficient associated with the function $\psi_{mnp}(R, \Theta, z)$ which is the mode function for the circular cylindrical interior, $\mathrm{J}_n(k_{np}R)$ is the Bessel function of nth order and k_{np} in the pth root of the transcendental equation $\mathrm{d}\mathrm{J}_n(k_{np}R)/\mathrm{d}R = 0$ at $R = 1$. This transcendental equation corresponds to the boundary condition (10). By way of construction, the velocity potential in equation (11) satisfies all the boundary conditions in the transformed domain, but not the governing equation.

We denote by $N_t = (M + 1) \times P \times (2N + 1)$ the total number of terms in the series expansion and define a global $N_t \times 1$ vector $\phi(t)$ consisting of all the expansion coefficients $\phi_{mnp}(t)$ in a proper order. Similarly, we define a global vector of expansion functions $\psi(R, \Theta, z)$ of size $N_t \times 1$ as

$$\phi(t) = \{\phi_{0(-N)1}, \ldots, \phi_{MNP}\}^{\mathrm{T}}, \qquad \psi(R, \Theta, z) = \{\psi_{0(-N)1}, \ldots, \psi_{MNP}\}^{\mathrm{T}}. \tag{12}$$

Equation (11) can now be written in the matrix form

$$\Phi(R, \Theta, z, t) = \psi^{\mathrm{T}}(R, \Theta, z)\phi(t). \tag{13}$$

Substituting equation (13) into equation (6), we can obtain the equation for the expansion coefficients as

$$\mathbf{A}\phi + \mathbf{B}\ddot{\phi} = \dot{\mathbf{q}}, \tag{14}$$

where the $N_t \times N_t$ matrix $\mathbf{A}$ is derived from the kinetic energy and is a generalized stiffness matrix. Similarly, the $N_t \times N_t$ matrix $\mathbf{B}$ is obtained from the potential energy and is the generalized mass matrix. The $N_t \times 1$ vector $\mathbf{q}$ refers to the set of generalized forces acting on the system due to the internal acoustic excitation.

2.4. MODAL ANALYSIS

Consider the free undamped solution $\phi(t) = \phi(\omega)\mathrm{e}^{\mathrm{j}\omega t}$. Equation (14) reduces to

$$[\mathbf{A} - \omega^2\mathbf{B}]\phi(\omega) = \mathbf{0}. \tag{15}$$

Let $\omega_i (i = 1, 2, \ldots, N_t)$ be the set of resonant frequencies of the acoustic medium obtained from equation (15) and ϕ_i the corresponding normalized eigen-vectors. Define the modal matrix $\mathbf{U} = \{\phi_1, \ldots, \phi_{N_t}\}$. Then we can show that

$$\mathbf{U}^{\mathrm{T}}\mathbf{B}\mathbf{U} = \mathbf{I}, \quad \mathbf{U}^{\mathrm{T}}\mathbf{A}\mathbf{U} = \mathbf{\Omega} = \mathrm{diag}(\omega_i^2). \tag{16}$$

The ith mode shape $\Phi_i(R, \Theta, z, t)$ corresponding to the frequency ω_i is given by

$$\Phi_i(R, \Theta, z, t) = \psi^{\mathrm{T}}(R, \Theta, z)\phi_i(t). \tag{17}$$

For the case of harmonically forced vibration $\mathbf{q}(t) = \mathbf{q}(\omega)\mathrm{e}^{\mathrm{j}\omega t}$, equation (14) is reduced to

$$[\mathbf{A} - \omega^2\mathbf{B}]\phi(\omega) = \mathrm{j}\omega\mathbf{q}(\omega). \tag{18}$$

Using equation (16) and introducing the transformation $\phi = \mathbf{U}\mathbf{y}$, we obtain a set of uncoupled equations for $\mathbf{y}$,

$$[\mathbf{\Omega} - \omega^2\mathbf{I}]\,\mathbf{y} = \mathrm{j}\omega\mathbf{U}^{\mathrm{T}}\mathbf{q}(\omega). \tag{19}$$

The vector $\mathbf{y}$ can be obtained in closed form for a general excitation $q(\mathbf{r}, t)$. After obtaining $\mathbf{y}$ and ϕ, the total forced acoustic response in the shell in the time domain is given by equation (13). The pressure distribution for both the free as well as the forced acoustic response can be computed from the velocity potential Φ using equation (1).

2.5. A NOTE ON COMPUTATION

Recall that the mapping of the z-co-ordinate is identity. The acoustic solution along the z-co-ordinate is separable from the (R, Θ) co-ordinates. Furthermore, the boundary conditions in the z direction are unchanged by the conformal mapping. We can show that $\cos(m\pi z/L)$ is still the component of the modal function in the transformed domain. Therefore, the orthogonality is preserved in the z direction when the expansion in equation (11) is used. As a result, the matrices $\mathbf{A}$ and $\mathbf{B}$ have a black-diagonal structure. For example, the matrix $\mathbf{A}$ can be written as

$$\mathbf{A} = \begin{bmatrix} \mathbf{A}_0 & & & \\ & \mathbf{A}_1 & & \\ & & \ddots & \\ & & & \mathbf{A}_M \end{bmatrix}, \tag{20}$$

where $\mathbf{A}_m$ $(m = 0, 1, \ldots, M)$ is a square matrix of dimension $(2N + 1) \times P$, and is associated with the function $\cos(m\pi z/L)$ for a given m. Because of the block-diagonal form, we can conduct the modal analysis, and calculate the acoustic responses in a block-by-block manner. The memory requirement for computing the acoustic response with many expansion terms is thus substantially reduced. The speed of computation is consequently enhanced.

This block-by-block computation ensures that the various sets of resonant frequencies for different longitudinal modes m are independent of each other. The number of longitudinal terms M does not effect the convergence of resonant frequencies in each individual block m. Figure 3 shows an example of the convergence of the resonant frequency of the mode

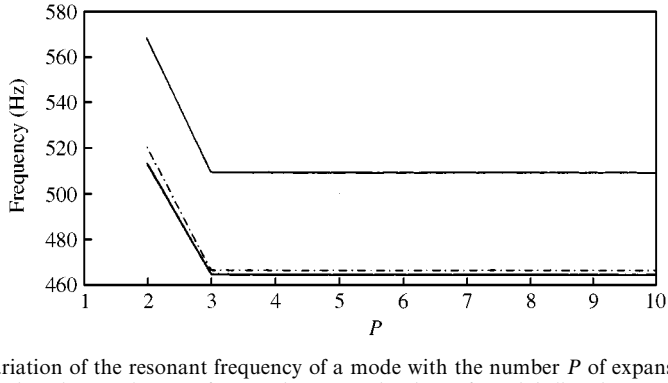

Figure 3. The variation of the resonant frequency of a mode with the number P of expansion terms in radial direction, while keeping the number N of expansion terms in circumferential direction constant. The mode is dominated by the expansion function with indices $n = -3$, $p = 2$, $m = 0$: (—), $N = 10$; (– · –), $N = 5$; (—), $N = 3$.

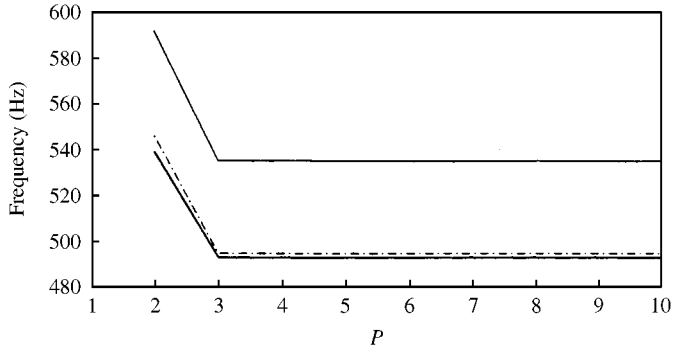

Figure 4. The variation of the resonant frequency of a mode with the number P of expansion terms in radial direction, while keeping the number N of expansion terms in circumferential direction constant. The mode is dominated by the expansion function with indices $n = -3$, $p = 2$, $m = 5$: (—), $N = 10$; (– · –), $N = 5$; (—), $N = 3$.

dominated by the expansion function with indices $n = -3$, $p = 2$, and $m = 0$. The number of terms in the radial direction P is increased from 1 to 10 while the number of terms in the circumferential direction N is kept constant. The figure shows the cases with $N = 3$, 5 and 10. It can be seen from the figure that the resonant frequency of this mode quickly converges as the number of terms in the expansion is increased. Similar convergence trends have also been observed for the modes with $m > 0$. To illustrate this, Figure 4 shows the convergence of the mode dominated by the expansion function with indices $n = -3$, $p = 2$, and $m = 5$. The resonant frequency of this mode also converges as the number of terms is increased.

Since the expansion function given in equation (11) leads to the Fourier series solution of the acoustic problem, the convergence of the solution with respect to the number of expansion terms is well known. In applying the Rayleigh–Ritz method, we need to choose the number of expansion terms for the solution. This is commonly done in the area of structural dynamics by considering the frequency bandwidth of interest. One chooses the number of expansion terms such that all the acoustic modes with resonant frequencies fall in the bandwidth, and makes sure that these modes are accurately approximated by adding additional expansion terms.

3. NUMERICAL RESULTS

Next, we present numerical results to demonstrate the application of the method. The cylindrical shell under considerations is 5 m long and has a $2 \times 2\ \mathrm{m}^2$ cross-section with rounded corners of radius 0·61 m. This corner radius corresponds to the parameter $k = 0{\cdot}75$ as can be seen from Figure 2. The air density is $\rho = 1{\cdot}023\ \mathrm{kg/m}^3$ and the speed of sound in the air is $c_0 = 330$ m/s.

3.1. MODE SHAPES OF ACOUSTIC PRESSURE

The numbers of expansion terms in this example are chosen as $M = 10$, $N = 5$ and $P = 5$ to demonstrate the method. The mode shapes of the acoustic pressure are presented at the cross-section $z = L/\sqrt{2}$.

Figure 5 shows the real and imaginary parts of the normalized mode shapes for the acoustic pressure $p_i(R, \Theta, z, t) = -\rho j\omega\Phi_i(R, \Theta, z, t)$ at the resonant frequency 91·25 Hz. The

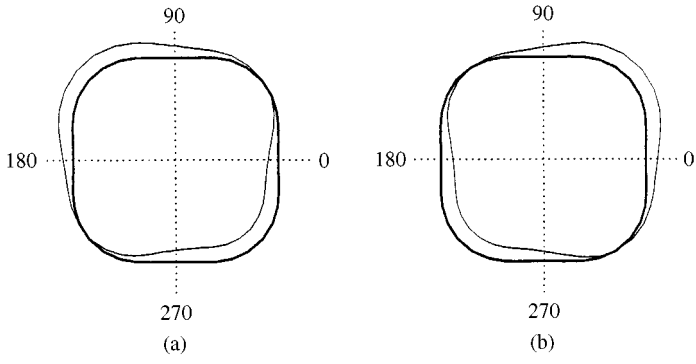

Figure 5. The mode shapes of the acoustic pressure at the resonant frequency 91·25 Hz. The thick line outlines the boundary of the cross-section while the thin line is the mode shape. The pressure is in Pascal, and is scaled for proper visualization around the physical domain. This is done for all other figures of mode shapes in the paper: (a) real part,(b) imaginary part.

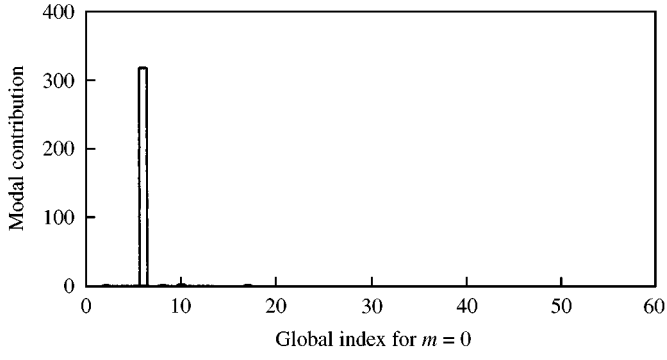

Figure 6. The contribution of the expansion coefficients to the modal vector at the resonant frequency 91·25 Hz.

modal vector that describes the contribution of the expansion functions to this mode is shown in the form of a bar graph in Figure 6. The 6th function with indices $m = 0$, $p = 1$ and $n = 1$ is dominant at this frequency. Note that there is a phase shift of $\pi/2$ between the real and the imaginary parts of the mode shapes. This is true for the several mode shapes presented later. The real and imaginary parts of the mode shapes of a circular cylindrical shell at the resonant frequency 96·70 Hz are shown in Figure 7. This mode shape is calculated using the same computer program as for the non-circular shell. The conformal mapping in this case is selected to be an identity. The modal contribution to this mode shape also shows the 6th function to be dominant with the indices $m = 0$, $p = 1$ and $n = 1$ similar to that in Figure 6. It is observed that the mode shape in the non-circular cylindrical shell is similar to the corresponding mode shape in the circular cylinder except for slight distortions at the corners.

The mode shapes at a resonant frequency of 349·76 Hz are shown in Figure 8. Figure 9 represents the modal contribution of the expansion functions to this mode. Note that the dominant functions in this case are represented by the set of indices $m = 0$, $p = 1$ and $n = \pm 2$. There are also contributions from the functions corresponding to the indices $m = 0$, $p = 2$ and $n = \pm 2$. Figure 10 shows the mode shapes at a resonant frequency of 396·17 Hz. Figure 11 represents the modal contribution of the expansion functions to this mode. The dominant functions correspond to the set of indices $m = 1$, $p = 1$ and $n = \pm 3$.

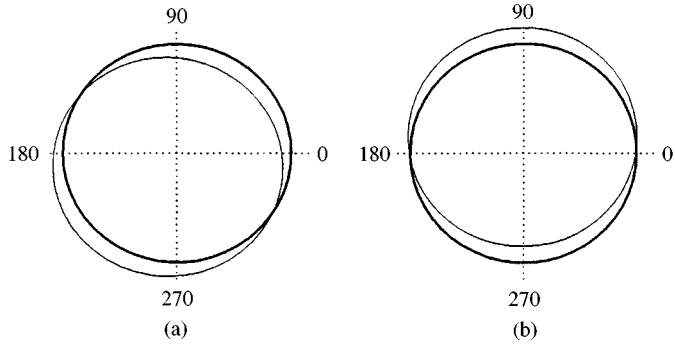

Figure 7. The mode shapes of the acoustic pressure in a circular cylindrical shell at the resonant frequency 96·70 Hz. The thick solid line outlines the cross-section of the shell while the thin solid line represents the mode shape: (a) real part, (b) imaginary part.

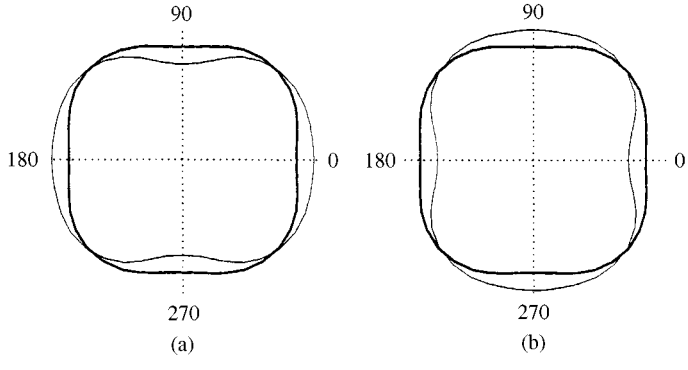

Figure 8. The real and imaginary parts of the mode shape of the acoustic pressure with the resonant frequency 349·76 Hz. The mode shapes are represented by the thin line and the cross-section of the shell is shown by the thick line: (a) real part, (b) imaginary part.

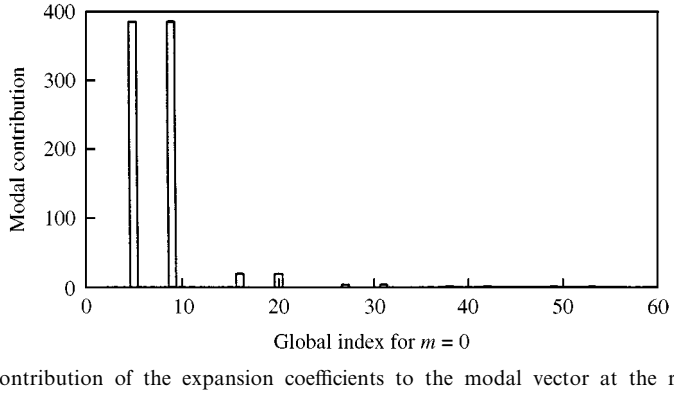

Figure 9. The contribution of the expansion coefficients to the modal vector at the resonant frequency 349·76 Hz.

There are also contributions from the functions corresponding to the indices $m = 1$, $p = 3$ and $n = \pm 1$.

Because the mapping in the z direction is identity, and because $\cos(m\pi z/L)$ is part of the true mode function of the system, the mode shapes in the z direction are the same as the function $\cos(m\pi z/L)$ and are not graphically shown in the paper.

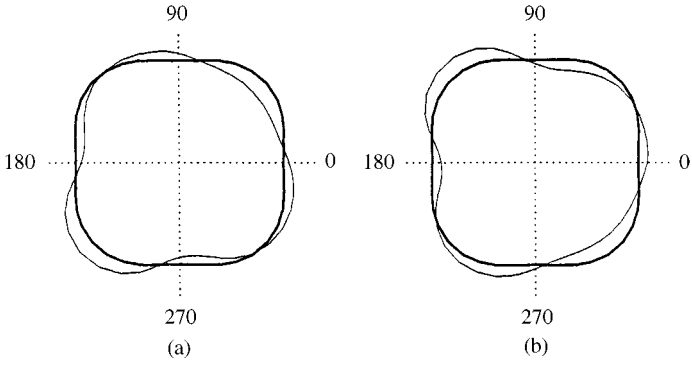

Figure 10. The real and imaginary parts of the mode shape of the acoustic pressure with the resonant frequency 396·17 Hz. The mode shapes are represented by the thin line and the cross-section of the shell is shown by the thick line: (a) real part, (b) imaginary part.

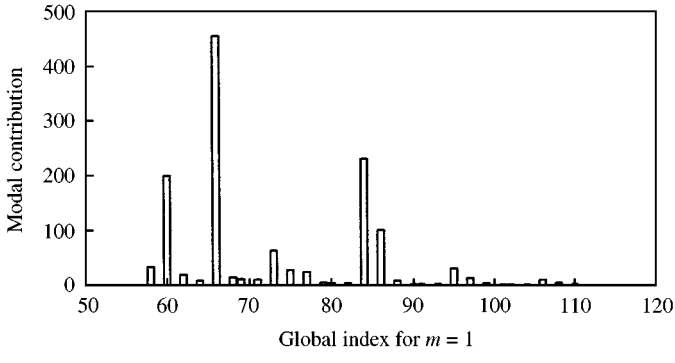

Figure 11. The contribution of the expansion coefficients to the modal vector at the resonant frequency 396·17 Hz.

3.2. FORCED RESPONSE

The excitation source considered in this paper is in the form of a point volume displacement within the enclosure. This can be expressed mathematically as [22]

$$q(\mathbf{r}, t) = q_0(\omega)\mathrm{e}^{\mathrm{j}\omega t}\delta(\mathbf{r} - \mathbf{r}_0), \tag{21}$$

where $\mathbf{r}_0$ refers to the position of the source. For all the simulations in this section, the source is assumed to be at the position $r = 0{\cdot}75$ m, $\theta = \pi/4$ and $z = L/\sqrt{2}$ in the physical domain. The magnitude of the excitation source is given by $q_0(\omega) = 1\ \mathrm{m}^3$. The forced response is computed along the curved boundary of the shell at the cross-section $z = L/\sqrt{2}$.

In the study of the forced response of the system, the variation of the pressure over a range of frequencies is analyzed. Figure 12 represents the frequency response of the pressure at $r = 1{\cdot}12$ m, $\theta = \pi/4$ and $z = L/\sqrt{2}$. The sound pressure level (SPL) is in dB referenced to 20 μPa. The various peaks and valleys in the graph represent the resonant and anti-resonant frequencies respectively. The spatial distribution of the forced acoustic pressure response is computed at a few of these frequencies.

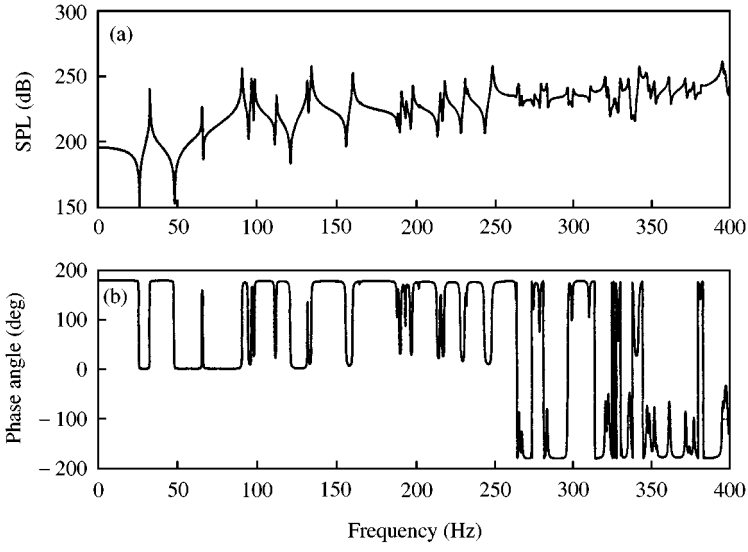

Figure 12. The frequency response function of the forced acoustic pressure: (a) magnitude of the sound pressure level in dB re 20 μPa and (b) phase angle.

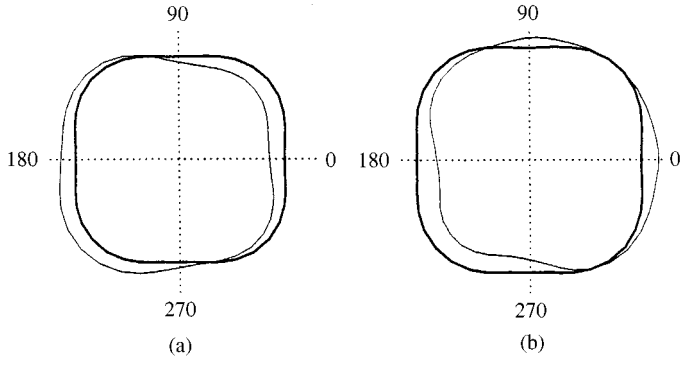

Figure 13. (a) The spatial distribution of the forced pressure response in Pascal at the resonant frequency 160·5 Hz. The dominant mode in this case has the indices $m = 0$, $p = 1$ and $n = \pm 1$. (b) The forced response pressure distribution at the anti-resonant frequency 156·2 Hz. The thick solid line represents the cross-section of the shell while the acoustic response is represented by the thin solid line. The pressure is scaled for proper visualization around the physical domain.

Figure 13 shows the forced pressure response at the resonant and anti-resonant frequencies: 160·5 and 156·2 Hz respectively. The response at the resonant frequency is dominated by the modes with $m = 0$, $p = 1$ and $n = \pm 1$. The pressure distribution is symmetrical with respect to the radial axis at $\theta = \pi/4$ where the excitation source is located. The response at the anti-resonant frequency contains contribution from a number of acoustic modes. As a result, the spatial distribution of the response does not resemble any acoustic mode shape.

The spatial distributions of the forced pressure response at the resonant frequency 320·5 Hz and the anti-resonant frequency 321·5 Hz are shown in Figure 14. The response at the resonant frequency is dominated by the acoustic mode shape with $m = 0$, $p = 2$ and $n = \pm 2$. At the anti-resonant frequency 321·5 Hz, the response again consists of contributions from several modes and is distorted.

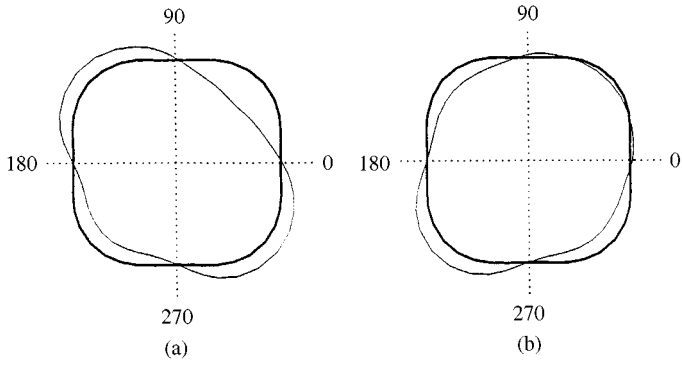

Figure 14. (a) The spatial distribution of the forced pressure response in Pascal at the resonant frequency 320·5 Hz. The dominant mode has the indices $m = 0$, $p = 2$ and $n = \pm 2$. (b) The forced response pressure distribution at the anti-resonant frequency 321·5 Hz. The thick solid line represents the cross-section of the shell while the acoustic response is represented by the thin solid line. The pressure is scaled for proper visualization around the physical domain.

4. CONCLUDING REMARKS

The free and forced acoustic response inside cylindrical shells with a non-circular cross-section has been studied. The solution method uses a conformal mapping to transform the non-circular domain into a circular one. The available mode functions for the circular domain are used as comparison functions in the Fourier series expansion for the solution of the original acoustic problem. The convergence of the Fourier series solution has been well established. In order to further assess the accuracy of the results, one must compare them with solutions obtained from different methods such as the finite element analysis or with experimental results. Such a comparative study is beyond the scope of this paper.

ACKNOWLEDGMENTS

This work is supported by a grant (F49620-98-1-0384) from the Air Force Office of Scientific Research.

REFERENCES

1. J. R. VINSON and K. POTTY 1995 *The Proceedings of the* 3*rd International Conference on Sandwich Constructions, Southampton.* Behavior of composite material sandwich rings and shells sections in complex structures.
2. K. P. K. POTTY and J. R. VINSON 1996 *in the Proceedings of the* 11*th Technical Conference of the American Society for Composites, Atlanta, GA.* Circumferential and radial behavior of anisotropic shells of variable cross-section.
3. K. SUZUKI, G. SHIKANAI, and A. W. LEISSA 1996 *International Journal of Solids and Structures*, **33**, 4079–4100. Free vibrations of laminated composite non-circular thick cylindrical shells.
4. J. M. M. HERNANDEZ *Advances in Acoustics Technology* 1995. New York: John Wiley and Sons.
5. E. H. MANSFIELD *The Bending and Stretching of Plates* 1964. Oxford: Pergamon Press.
6. T. IRIE, G. YAMADA, and M. SONODA 1983 *Journal of Sound and Vibration* **86**, 442–448. Natural frequencies of square membrane and square plate with rounded corners.
7. N. I. MUSKHELISHVILI 1953 *Some Basic Problems of the Mathematical Theory of Elasticity.* Groningen, Holland: P. Noordhoff Ltd.

8. M. M. BANERJEE 1976 *Journal of Applied Mechanics* **43E**, 356–357. Note on the large deflections of irregular shaped plates by the method of conformal mapping.
9. A. C. STEVENSON 1943 *Philosophical Magazine* **34**, 105–114. The boundary couples in thin plates.
10. P. THAMBURAJ and J. Q. SUN 2000 *Journal of Sandwich Structures and Materials*. Modal analysis of a non-circular cylindrical laminated shell using conformal mapping. In Review.
11. P. THAMBURAJ and J. Q. SUN 2000 *Proceedings of Nonlinear Vibrations, Stability, and Dynamics of Structures, Blacksburg, VA, U.S.A.* Vibrations of a non-circular cylindrical shell using conformal mapping.
12. P. A. A. LAURA 1964 *Journal of the Royal Aeronautical Society* **68**. On the determination of the natural frequency of a star-shaped membrane.
13. P. A. A. LAURA, C. E. GIANETTI, R. H. GUTIERREZ and L. DIEZ 1978 *Journal of Sound and Vibration* **60**, 499–509. Determination of eigenvalues in a class of doubly connected regions in problems governed by Helmholtz's equation.
14. B. S. BERGER. 1978 *Journal of Applied Mechanics* **45**, 149–152. Transient motion of an elastic shell of revolution in an acoustic medium.
15. R. SCHINZINGER and P.A.A. LAURA 1991. *Conformal Mapping: Methods and Applications*. New York, U.S.A. Elsevier.
16. P. A. A. LAURA 1967 *The Journal of the Acoustical Society of America*, **42**, 21–26. Calculations of eigenvalues for uniform fluid waveguides with complicated cross sections.
17. M. J. HINE 1971 *Journal of Sound and Vibration* **15**, 295–305. Eigenvalues for a uniform fluid waveguide with an eccentric-annulus cross-section.
18. P. A. A. LAURA, E. ROMANELLI and M. J. MAURIZI 1972 *Journal of Sound and Vibration* **20**, 27–38. On the analysis of waveguides of doubly-connected cross-section by the method of conformal mapping.
19. D. T. DIPERN and T. K. STANTON 1994 *The Journal of the Acoustical Society of America* **96**, 3064–3079. Sound scattering by cylinders of noncircular cross section: A conformal mapping approach.
20. G. M. L. GLADWELL and G. ZIMMERMANN 1966 *Journal of Sound and Vibration* **3**, 233–241. On energy and complementary energy formulations of acoustic and structural vibration problems.
21. G. M. L. GLADWELL 1966 *Journal of Sound and Vibration* **4**, 172–186. A variational formulation of damped acousto-structural vibration problems.
22. F. FAHY 1985 *Sound and Structural Vibration–Radiation, Transmission and Response*. New York: Academic Press.
23. E. H. DOWELL, G. F. GORMAN III and D. A. SMITH 1977 *Journal of Sound and Vibration* **52**, 519–542. Acoustoelasticity: General theory, acoustic natural modes and forced response to sinusoidal excitation, including comparison with experiment.
24. L. MEIROVITCH 1967 *Analytical Methods in Vibrations*. New York: Macmillan.
25. M. D. GREENBERG 1998 *Advanced Engineering Mathematics*. Upper Saddle River, NJ: Prentice-Hall.